Ferromagnetic resonance of Co thin films grown by atomic layer deposition on the Sb_2Te_3 topological insulator

Emanuele Longo[†‡], Claudia Wiemer[†], Matteo Belli [†], Raimondo Cecchini[†], Massimo Longo[†], Matteo Cantoni[Δ], Christian Rinaldi[Δ], Michael D. Overbeek[#], Charles H. Winter[#], Gianluca Gubbiotti[°], Graziella Tallarida[†], Marco Fanciulli[†‡] and Roberto Mantovan[†*]*

[†]CNR-IMM, Unit of Agrate Brianza (MB), Via C. Olivetti 2, 20864, Agrate Brianza (MB), Italy

[‡] Università degli studi di Milano-Bicocca, Dipartimento di Scienze dei Materiali, Via R. Cozzi 55,20126, Milano, Italy

[Δ]Dipartimento di Fisica, Politecnico di Milano, Via G. Colombo 81, 20131 Milano, Italy

[°] Istituto Officina dei Materiali del CNR (CNR-IOM), Sede Secondaria di Perugia, c/o Dipartimento di Fisica e Geologia, Università di Perugia, I-06123 Perugia, Italy

[#]Winter Laboratory, Wayne State University, 48202 Cass Ave, Detroit (MI), U.S.A.

Corresponding authors:

e-mail: Emanuele.Longo@mdm.imm.cnr.it

e-mail: Roberto.Mantovan@mdm.imm.cnr.it

Abstract

Interfacing ferromagnetic materials with topological insulators is an intriguing strategy in order to enhance spin-to-charge conversion mechanisms, paving the way toward highly efficient spin-based electronic devices. In particular, the use of large-scale deposition techniques is demanding for a sustainable and cost-effective industrial technology transfer. In this work, we study the magnetic properties of the Co/Sb_2Te_3 heterostructure, where the ferromagnetic Co layer is deposited by atomic layer deposition on top of the Sb_2Te_3 topological insulator, which is grown by metal organic chemical vapor deposition. In particular, broadband ferromagnetic resonance is employed to characterize the Co/Sb_2Te_3 system and the reference heterostructure Co/Pt. For Co/Sb_2Te_3, we extract an effective magnetic anisotropy constant $K_{eff} = 4.26 \cdot 10^6 \frac{erg}{cm^3}$, which is an order of magnitude higher than in Co/Pt ($K_{eff} = 0.43 \cdot 10^6 \frac{erg}{cm^3}$). The large difference in the K_{eff} values observed in Co/Sb_2Te_3 and Co/Pt is explained in terms of the different Co crystalline structures achieved on top of Sb_2Te_3 and Pt, respectively. Interestingly, the Co/Sb_2Te_3 system displays a relatively large Gilbert damping constant ($\alpha = 0.095$), which we suggest as possibly due to spin pumping from the Co layer into the Sb_2Te_3 topological insulator.

I. Introduction

The coupling between ferromagnetic thin films (FM) and topological insulators (TI) is attracting huge interest in the context of spintronics [1,2]. Indeed, the presence of Dirac-like dispersed surface states in the TI, jointly with the large spin-orbit coupling, is expected to favor a super-efficient magnetization manipulation of the FM through a large *spin orbit torque* (SOT) [3].

Here, we present the use of a pure Atomic Layer Deposition (ALD) process to grow Co thin films in direct contact with the Sb_2Te_3 TI layer, as grown by Metal Organic Chemical Vapor Deposition (MOCVD) [4,5]. Both ALD and MOCVD allow deposition processes on a large scale that could favour the future technology-transfer. In particular, ALD has been scarcely employed so far in the context of spintronics [6–8]. The ALD of FMs is very appealing since it could provide highly controllable and conformal growth on top of even granular TIs [4,5]. The ALD of Co thin films is conducted by varying the layers thickness from few to tens of nm on top of granular Sb_2Te_3 films. Simultaneously, at each nominal thickness, the ALD of Co is conducted on top of Pt (grown by magnetron sputtering). The reason for that is that Pt is the workhorse heavy metal (HM) material for SOT applications [9], thus providing an interesting reference to conduct a comparison between Co/Sb_2Te_3 and Co/Pt in terms of magnetic properties.

By X-ray diffraction (XRD) measurements, we observe the formation of different Co polymorphs depending on the underlying material, with the Co layers showing the hexagonal crystalline (hcp) and face-centered cubic (fcc) structures on top of Sb_2Te_3 and Pt, respectively. The systems are compared in terms of their magnetocrystalline (MC) anisotropy properties by employing Broadband Ferromagnetic Resonance (BFMR), with complementary information obtained by Magnetic Force Microscopy (MFM) and Vibrating Sample Magnetometry (VSM).

We find that the Co/Sb_2Te_3 system displays an anisotropy constant $\mathrm{K}_{eff} = 4.26 \cdot 10^6 \frac{erg}{cm^3}$, being one order of magnitude higher than the value we measured for Co/Pt, thus showing that the simultaneous ALD of Co on top of Sb_2Te_3 and Pt can provide a method to tune the magnetic anisotropy depending on the substrate. Interestingly, for the Co(8.1 nm)/Sb_2Te_3 system we extract a Gilbert damping of $\alpha = 0.095$. This value is much higher than that typically reported for the Co/Pt heterostructures [10], suggesting possible spin-pumping mechanisms in the granular Sb_2Te_3 topological insulator [10,11].

II. Materials and Methods

A 35 nm-thick, polycrystalline and electrically continuous Sb_2Te_3 thin film was deposited by Metal Organic Chemical Vapor Deposition (MOCVD) on a 4 inch SiO_2(50 nm)/Si substrate at room temperature (RT). The film shows a granular structure characterized by a root mean square roughness of 2-5 nm. The topological behaviour of the as-deposited Sb_2Te_3 layers has been previously validated through magnetotransport studies evidencing weak antilocalization (WAL) effects [4].

Uncoated 70 nm thick Pt layers were grown on top of SiO_2(100 nm)/Si(100) substrates sputtered with 3 kV argon ions.

The ALD of metallic Co on top of both Sb_2Te_3 and Pt, was carried out at the fixed temperature of 180°C with an industrial Picosun R-200 BE reactor for thermal ALD, connected to a house N_2 source and equipped with a SAES in-line purifier for a 99.99999% N_2 quality. Further details about the adopted ALD recipe can be found in Ref.[12] and [14].

Table 1 summarizes the two sets of samples that were produced with the indicated number of ALD cycles [14]. For each nominal process (i.e. number of ALD cycles), the ALD was conducted simultaneously on top of Sb_2Te_3 and Pt samples, and the obtained Co thicknesses (as measured by XRR) are summarized in *Table 1* for both Sb_2Te_3 and Pt-based heterostructures.

Table 1: List of the Co layer thickness values for Co/Sb_2Te_3 and Co/Pt sets of samples as a function of the number of ALD cycles, expressed in nm.

Number of ALD Cycles	Co thickness in Co/Sb_2Te_3 (nm)	Co thickness in Co/Pt (nm)
100	3.5	1.8
250	8.1	6.3
1000	50	35

All the samples were studied by Grazing Incidence X-Ray Diffraction (GIXRD). GIXRD patterns were acquired using a four-circle diffractometer equipped with a position-sensitive gas detector (Inel CPS-120). In all measurements, the angle of incidence between the X-ray beam and the sample was fixed at $\omega = 2°$ [13]. The structural continuity, the electronic density and the roughness of each layer were determined by XRR analysis [14], confirming the high quality of the

Co/Sb_2Te_3 heterostructure. In particular, the root mean square roughness of each layer was 3.5 nm and 2.3 nm, respectively for Co and Sb_2Te_3. Further details about the chemical-structural properties of the Co/Sb_2Te_3 heterostructure are reported in Ref. [14].

Magnetic force microscopy (MFM) measurements were performed at the Co surface of the Co/Sb_2Te_3 heterostructures with a Bruker AFM/MFM commercial system. In order to efficiently decouple the magnetic and morphological signals during each MFM acquisition, the tip was maintained at 200 nm distance from the sample surface.

The heterostructures hysteresis loops were recorded through a MicroSense EZ-9 vibrating sample magnetometer (VSM), from which we extracted the saturation magnetization (M_s) and identified the magnetization's easy axis.

The FMR measurements were performed using a home-made facility obtained from the customization of a Bruker ER-200 instrument originally adopted for Electron Paramagnetic Resonance (EPR) measurements. As a microwave generator, it was used a broadband Anritsu-MG3694C source. The microwave source was connected to a custom-made U-shaped grounded coplanar waveguide (GCPW) fabricated through photolithography on a Taconic RF-35 material made by a Cu(350 µm)/Insulator/Cu(350 µm) multilayer developed for high-frequency purposes. The samples were accommodated face down on the GCPW (FM layer close to the GCPW surface) with a 20 µm-thick Mylar foil placed in between. The GCPW was connected to both the Anritsu source and the Anritsu-ML2488A/B power meter, in order to measure the signal power passing through the board (transmission configuration). *Figure 1* shows the image of the GCPW, with the Co/Sb_2Te_3 sample visible across the board signal lines.

Figure 1: Image of the home-made U-shaped GCPW, where a Co/Sb_2Te_3 sample is glued across the signal line. A small piece of mylar foil is positioned between the sample and the board in order to avoid electrical shortening of the line.

The FMR measurement was conducted positioning the sample between the polar extensions of the Bruker ER-200 electromagnet and maintaining its surface parallel to the external magnetic field, in the so-called in-plane (IP) configuration. Once the microwave frequency was fixed, the measurement was performed by measuring the absorption power downstream the electrical transmission line as a function of the external magnetic field. The same procedure was repeated for different frequency values.

III. Results and Discussion

Figure 2 displays the GIXRD patterns of Co(50 nm)/Sb_2Te_3 and Co(35 nm)/Pt. In *Fig 2 (a)*, the position and the sharpness of the Sb_2Te_3 peaks as compared to the powder reference evidence the high crystallinity of this granular film, which is also characterized by a

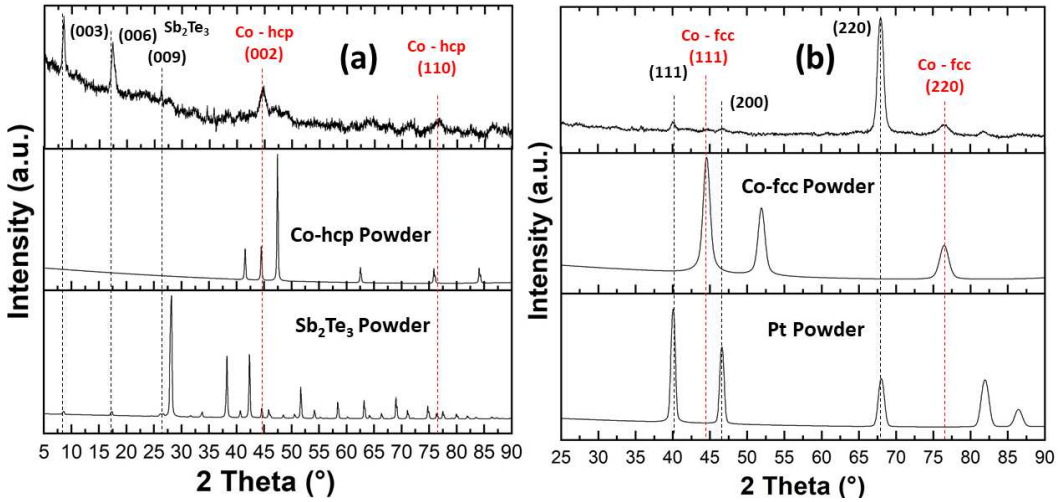

Figure 2: GIXRD pattern for Co(50 nm)/Sb_2Te_3 (a) and Co(35 nm)/Pt (b). The Co-hcp and Co-fcc crystalline phases were identified respectively on the Sb_2Te_3 and the Pt substrates.

preferential out-of-plane (OOP) orientation along the [00 ℓ] direction [5]. Here, the positions of the Co peaks at $2\Theta{\sim}45°$ and $2\Theta \sim 75°$ (see red dotted line in *Fig.2(a)*), correspond respectively to the (002) and the (110) reflections of the hcp Co phase. From *Fig. 2(b)*, the cubic Pt substrate results crystalline and with a preferred OOP grains orientation along the [111] direction. On top of Pt, the Co diffraction pattern is clearly different than that shown in Fig.2(a), being now the most intense reflection positioned at $2\Theta{\sim}76°$. This shows that the Co crystalline structure on top of Pt is fcc.

We recently reported about the interface chemical composition and microstructure of the Co/Sb_2Te_3 heterostructure [14]. In particular, using High-Resolution Transmission Electron Microscopy (HRTEM) and Energy Dispersive X-ray Spectroscopy (EDS) on a cross sectional lamella of a $Co(8.1\ nm)/Sb_2Te_3$ sample, we evidenced a very high conformality of the Co layer on top of the Sb_2Te_3 substrate, showing an almost absent intermixing at the interface. The magnetic properties discussed in the following are therefore connected to a pure Co/Sb_2Te_3 interface, in the absence of secondary phases and/or major structural defects at the interface.

In *Figure 3,* the MFM images of the Co/Sb_2Te_3 stacks are shown. As it is evident from a qualitative comparison among the three acquisitions, the sample with the thicker Co (50 nm) film (*Fig. 3(a)*) shows the strongest magnetic contrast and the largest magnetic domain size (few µm). In *Figure 3(b)* the size of the magnetic domains is reduced to hundreds of nm with a consequent lowering of the magnetic contrast. In the case of the thinnest sample the magnetic contrast disappeared, likely indicating the almost-full oxidation of the Co (3.5 nm) layer. In the following, we focus our attention on the thinnest Co layers showing magnetic contrast, i.e. the sample shown in *Fig.3(b)*.

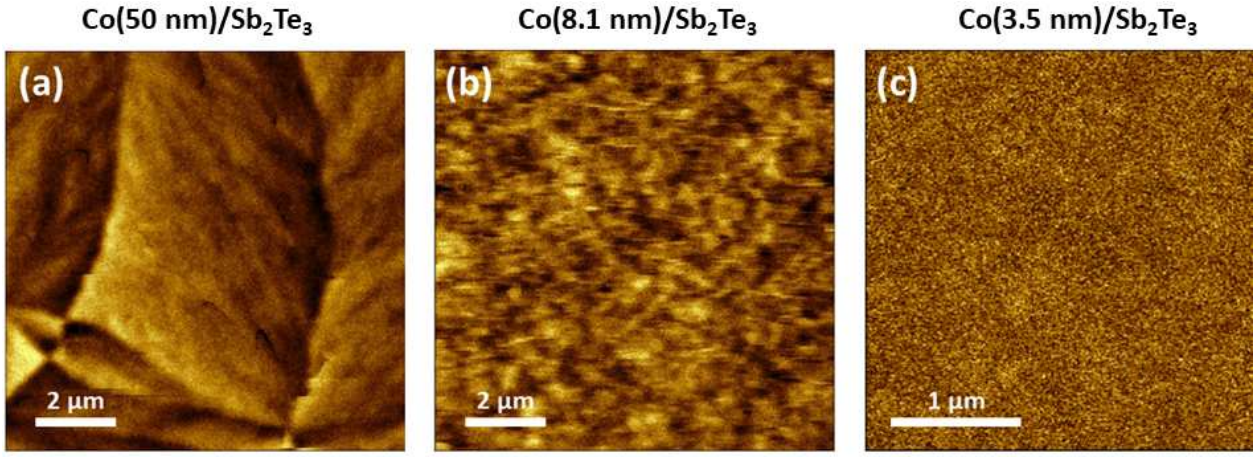

Figure 3: MFM measurements for the Co/Sb_2Te_3 samples. (a) The Co (50 nm) is characterized by a strong magnetic contrast with very sharp magnetic domains few µm large; (b) the thinner Co (8.1 nm) film evidences a weaker magnetic contrast as compared with (a), with a reduced magnetic domains size of hundreds of nanometers. (c) In this sample no magnetic contrast was evidenced, likely due to the complete oxidation of the Co layer.

It is know that the magnetic properties of Co-hcp and Co-fcc are different as due to the different crystal symmetry [10,15,16]. In the following, we present our investigation on the magnetic anisotropy properties of the developed Co/Sb_2Te_3 and Co/Pt systems.

Figure 4 shows the *M(H)* curves of the Co(8.1 nm)/Sb_2Te_3 and Co(6.3 nm)/Pt samples (*Table 1*), as measured by VSM with the external magnetic field oriented along the film plane. Both samples clearly show an in-plane easy axis. The extracted values for the saturation magnetization (M_S) are $M_S = 922 \frac{emu}{cm^3}$ for the Co-hcp/Sb_2Te_3 sample and $M_S = 612 \frac{emu}{cm^3}$ for the Co-fcc/Pt , being compatible with those reported for chemically-grown Co thin films [18], and slightly lower than for the bulk Co-hcp and Co-fcc. The lower M_S in thin films, when compared to the bulk

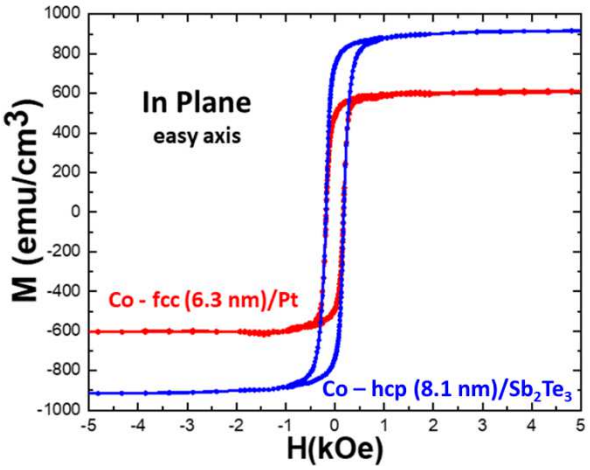

Figure 4: In-plane VSM measurements on the Co(8.1 nm)/Sb_2Te_3 (blue line) and the Co(6.3 nm)/Pt (red line) samples.

counterpart, is mainly attributed to the presence of magnetic dead layers at the Co surface, which are certainly present in in our samples, due to the absence of any capping layer. From the thorough structural analysis conducted on these systems, we know that the polycrystalline Co films exhibit a preferred OOP crystallographic orientation, which is the [00ℓ] direction for Co grains on Sb_2Te_3 and the [111] direction for Co on Pt substrates [14]. Therefore, we associate the hard axis of the magnetization to the [00ℓ] direction in the Co/Sb_2Te_3 structure and to the [111] direction in the Co/Pt samples, respectively. Importantly, as due to the polycrystalline nature of the underneath Sb_2Te_3 and Pt layers, no preferential orientation of the Co grains in the film plane has been observed, preventing us to correlate the easy axis direction with a specific orientation of the Co crystalline structure.

A magnetic anisotropy study has been carried out on samples Co(8.1 nm)/Sb_2Te_3 and Co(6.3 nm)/Pt through BFMR. The magnetization dynamics in a FM material is described by the Landau-Lifshitz-Gilbert (LLG) equation, which correlates the temporal variation of the magnetization ***M*** with the orientation of an external applied magnetic field ***H*** [15], see *Eq.1*.

$$\frac{d\boldsymbol{M}}{dt} = -\mu_0\gamma\boldsymbol{M}\times\boldsymbol{H} + \frac{\alpha}{M_s}(\boldsymbol{M}\times\frac{d\boldsymbol{M}}{dt}) \qquad [1]$$

The first factor on the right-hand side of *Eq.1* represents the precessional motion of ***M*** around the ***H*** direction and $\gamma = \frac{ge}{2m_e}$ is the gyromagnetic ratio, where *g* is the Landé factor, *e* the electron charge and m_e the effective mass of the electron in a solid. The second contribution to *Eq.1* includes all the dissipative effects as accounted with the so called *damping constant* (or *Gilbert parameter) α* [11].

For the IP configuration, from the LLG equation it is possible to derive the Kittel formula as expressed in *Eq.2*, which correlates the resonant frequency of the magnetization (f_{res}) with the resonant magnetic field (H_{res}). The square root trend of this curve makes extremely important to

$$f_{res}(H_{res}) = \frac{\gamma}{2\pi}\sqrt{H_{res}(H_{res}+4\pi M_{eff})} \quad [2]$$

have a large number of data points, in order to reduce as much as possible the errors on fitted parameters. In order to extract the H_{res} value, we fitted the FMR absorption line for a fixed frequency with the Lorentzian function reported in *Eq.3*, where *P(H)* on the Y-axis represents the microwave power absorbed by the sample for a specific f_{res} value. As an example, an FMR

$$P(H) = -A_a\frac{\Delta H(H-H_{res})}{(H-H_{res})^2+(\Delta H)^2} + A_s\frac{(\Delta H)^2}{(H-H_{res})^2+(\Delta H)^2} \qquad [3]$$

absorption line is reported in the inset of *Figure 5*, where H_{res} and the linewidth ΔH are indicated.

In the context of the LLG description, the damping parameter α plays a key-role in determining the magnetization dynamics properties in ferromagnetic materials [17], and consequently the measurement of α, and its engineering, are of interest in view of tailoring the magnetic devices functionalities. In a ferromagnetic material the α value is directly related to the linewidth ΔH of its FMR absorption line and linearly dependent on the excitation frequency according to the following equation [Eq.4].

where ΔH_0 represents the curve intercept, commonly attributed to structural and/or

$$\Delta H(f_{res}) = \frac{4\pi\alpha}{\gamma}f_{res} + \Delta H_0 \qquad [4]$$

magnetic inhomogeneities [18].

Figure 5 shows the $f_{res}\,(H_{res})$ data for the Co(8.1 nm)/Sb_2Te_3 (blue squares) and Co(6.3 nm)/Pt (red triangles) heterostructures. The BFMR data are fitted with the Kittel equation for the IP configuration [*Eq.2*], in order to extract the values for M_{eff}, which is defined by the relation $4\pi M_{eff} = 4\pi M_S - H_k$, where H_k the anisotropy field [15,19]. We measure $M_{eff}^{Co-hcp/Sb_2Te_3} = 554\,\frac{emu}{cm^3}$ and $M_{eff}^{Co-fcc/Pt} = 636\,\frac{emu}{cm^3}$. By substituting the M_S values obtained from the VSM measurements in the above relation, we finally obtain $H_k^{Co-hcp/Sb_2Te_3} = 4626\,Oe$ and $H_k^{Co-fcc/Pt} = -312\,Oe$.

The anisotropy field H_k can be written as $H_k = \frac{K_{eff}}{M_S}$, where K_{eff} is known as the effective anisotropy constant and takes into account the crystalline structure of a ferromagnetic material, which is intimately related to its magnetic properties [15,20]. From the literature, it is well known that Co-hcp and Co-fcc exhibit large differences in term of MC anisotropy, due to the different symmetries of their crystalline structures [21]. In general, when the relative orientation of ***M*** with respect to a specific crystalline plane is known, it is possible to expand K_{eff} as a series of multiple terms which contribute to the calculation of the free energy density for a certain crystal symmetry [15]. Being the preferential ***M*** orientation in a polycrystalline Co film not defined, we consider the total effective anisotropy constant K_{eff} as a marker of the different magnetic anisotropy

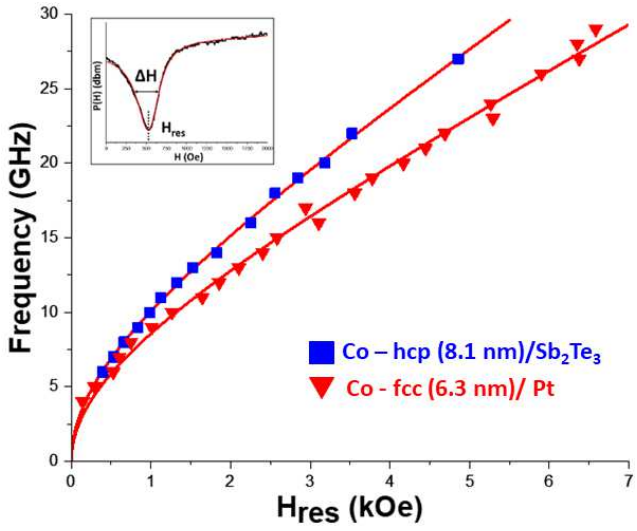

Figure 5: Field of resonance $f_{res}(H_{res})$ *of the Co(8.1 nm)/*Sb_2Te_3 *(blue squares) and Co(6.3 nm)/Pt (red triangles) samples for the IP FMR configuration. The red solid line represents the fitted data with Eq.2. The inset shows a typical FMR absorption curves, in which the resonant magnetic field* H_{res} *and the linewidth* ΔH *are indicated.*

characterizing the hcp and fcc Co polymorphs. We obtain $K_{eff}^{Co-hcp/Sb_2Te_3} = 4.26 \cdot 10^6 \frac{erg}{cm^3}$ and $K_{eff}^{Co-fcc/Pt} = 0.43 \cdot 10^6 \frac{erg}{cm^3}$. The Co-hcp phase on top of Sb_2Te_3 presents an order of magnitude higher K_{eff} value as compared the cubic Co on top of Pt, as it is expected when comparing hcp and fcc phases [21]. Complementary Brillouin Light Scattering (BLS) measurements have been conducted to confirm the validity of the BFMR collected data (*Supplementary Information*) [22,23].

Solely considering the shape anisotropy energy density (defined by $\frac{1}{2}\mu_0 M_s^2$), which is respectively $0.43 \cdot 10^6 \frac{erg}{cm^3}$ and $0.19 \cdot 10^6 \frac{erg}{cm^3}$ for Co-hcp/Sb_2Te_3 and Co-fcc/Pt, it is not possible to interpret the order of magnitude for the difference between the measured K_{eff} values, which is therefore mainly attributed to the different MC anisotropy. The BFMR results elegantly prove the possibility to tune the magnetism of ALD-Co thin films through an appropriate substrate selection.

From the data reported in *Fig.5*, the *g* factor values for the Co(8.1 nm)/Sb_2Te_3 and Co(6.3 nm)/Pt heterostructures are obtained, resulting in $g^{Co/Sb_2Te_3} = 2.4 \pm 0.2$ and $g^{Co/Pt} = 2.1 \pm 0.2$. As already mentioned, the IP configuration and the large width of the FMR absorption peaks make the determination of the H_{res} values in the low frequency region of *Fig.5* very challenging. This is the main reason for the relatively large error bars in determining the *g* factor values. On the other hand, by comparing these values with those already reported [24], we underline that g^{Pt} shows a

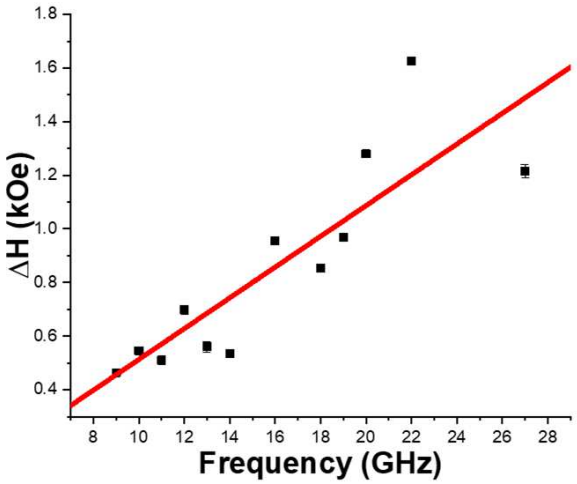

Figure 6: Frequency-dependent linewidth (ΔH) for the Co(8.1 nm)/Sb_2Te_3 heterostructure. The red line indicates the fit of the data with Eq.4.

good agreement. The apparent higher $g^{Sb_2Te_3}$ value will be the subject of further investigations, since according to *Beaujour et al.* [25], the increase of the *g* factor is attributed to a possible lowering of symmetry at the Co/Sb_2Te_3 interface, which can cause an enhancement of the $\mu_\ell/\mu_s = |g-2|/2$ ratio, where μ_ℓ and μ_s are the orbital and the spin moments, respectively [15]. Motivated by the observed enhancement of the *g* factor in the Co/Sb_2Te_3 heterostructure, in *Fig.6* we plotted the frequency-dependent linewidth for the Co(8.1 nm)/Sb_2Te_3 sample. Here, from the fit of the collected data with *Eq.4*, we extracted the values for the damping parameter α and for the inhomogeneous term ΔH_0.

Interestingly, we found that $\alpha^{Co(8.1\,nm)/Sb_2Te_3} = 0.095 \pm 0.04$. This is a considerably high value when compared to the intrinsic damping parameter (α_0) for pure Co, independently of its crystalline structure, which is usually reported as being in the range of $0.0052 - 0.0085$ [10]. Furthermore, this enhanced value has been found to be almost one order of magnitude higher also as compared to Co/Pt heterostructures, as reported by *Verhagen et al.* [26]. In several cases, the enhanced damping parameter has been attributed to a possible spin-pumping effect from the FM to adjacent non-magnetic (NM) layers. Indeed, Ref.[10] underlines how the intrinsic damping

of a FM could be influenced by a spin current flowing across the FM/NM interface, in terms of the spin-mixing conductance ($g_{\uparrow\downarrow}^{T,eff}$) of a multilayer heterostructure. This picture is reinforced by considering the TEM and EDS analysis of the Co/Sb_2Te_3 interface [14], which rules out the presence of secondary phases that could impede the successful spin pumping from Co to the Sb_2Te_3 topological insulator.

IV. Conclusion

We successfully employed a pure ALD process to grow Co thin films in contact with the MOCVD-grown granular topological insulator Sb_2Te_3 films. The Co growths were simultaneously carried out on top of Pt layers, in order to compare the Co/Sb_2Te_3 and Co/Pt stacks from the point of view of their magnetic anisotropy. The Co layers are found in the structural hcp and fcc phases, on top of Sb_2Te_3 and Pt respectively. By employing BFMR, we observed an order of magnitude higher anisotropy constant K_{eff} in Co-hcp/Sb_2Te_3 when compared to Co-fcc/Pt. This demonstrated the possibility to exploit ALD to engineer the magnetic anisotropy of Co thin films by controlling their crystalline structure through the appropriate substrate selection. As a preliminary - though intriguing – result, we also reported an enhanced Gilbert damping α parameter for Co/Sb_2Te_3 when compared to those typically reported for Co/Pt. As a possible origin for this damping enhancement, we suggest the spin pumping into the TIs, which will be the subject of future studies.

Acknowledgments

We acknowledge the *MP1402-Hooking together the European research in atomic layer deposition (HERALD) cost action* and the Horizon 2020 project SKYTOP "*Skyrmion-Topological Insulator and Weyl Semimetal Technology*" (FETPROACT-2018-01, n. 824123). Efforts at Wayne State University were supported by the *U.S. National Science Foundation* (Grant No. CHE-1607973) and *EMD Performance Materials*.

V. Bibliography

[1] A. Soumyanarayanan, N. Reyren, A. Fert, C. Panagopoulos, Emergent phenomena induced by spin–orbit coupling at surfaces and interfaces, Nature. 539 (2016) 509–517. https://doi.org/10.1038/nature19820.

[2] F. Hellman, A. Hoffmann, Y. Tserkovnyak, G.S.D. Beach, E.E. Fullerton, C. Leighton, A.H. MacDonald, D.C. Ralph, D.A. Arena, H.A. Dürr, P. Fischer, J. Grollier, J.P. Heremans, T. Jungwirth, A.V. Kimel, B. Koopmans, I.N. Krivorotov, S.J. May, A.K. Petford-Long, J.M. Rondinelli, N. Samarth, I.K. Schuller, A.N. Slavin, M.D. Stiles, O. Tchernyshyov, A. Thiaville, B.L. Zink, Interface-induced phenomena in magnetism, Reviews of Modern Physics. 89 (2017). https://doi.org/10.1103/RevModPhys.89.025006.

[3] A.R. Mellnik, J.S. Lee, A. Richardella, J.L. Grab, P.J. Mintun, M.H. Fischer, A. Vaezi, A. Manchon, E.-A. Kim, N. Samarth, D.C. Ralph, Spin-transfer torque generated by a topological insulator, Nature. 511 (2014) 449–451. https://doi.org/10.1038/nature13534.

[4] R. Cecchini, R. Mantovan, C. Wiemer, L. Nasi, L. Lazzarini, M. Longo, Weak Antilocalization in Granular Sb_2Te_3 Thin Films Deposited by MOCVD, Physica Status Solidi (RRL) - Rapid Research Letters. 12 (2018) 1800155. https://doi.org/10.1002/pssr.201800155.

[5] E. Longo, C. Wiemer, R. Cecchini, M. Longo, A. Lamperti, A. Khanas, A. Zenkevich, M. Fanciulli, R. Mantovan, Chemical, structural and magnetic properties of the Fe/Sb2Te3 interface, Journal of Magnetism and Magnetic Materials. 474 (2019) 632–636. https://doi.org/10.1016/j.jmmm.2018.12.009.

[6] R. Mantovan, S. Vangelista, B. Kutrzeba-Kotowska, S. Cocco, A. Lamperti, G. Tallarida, D. Mameli, M. Fanciulli, Synthesis of magnetic tunnel junctions with full in situ atomic layer and chemical vapor deposition processes, Thin Solid Films. 520 (2012) 4820–4822. https://doi.org/10.1016/j.tsf.2011.08.037.